A metabolomic and systems biology perspective on the brain of the Fragile X syndrome mouse model

Laetitia Davidovic,[1,2,8] Vincent Navratil,[3,4] Carmela M. Bonaccorso,[5] Maria Vincenza Catania,[5,6] Barbara Bardoni,[1,2] and Marc-Emmanuel Dumas[3,7,8]

[1]*Institut de Pharmacologie Moléculaire et Cellulaire, CNRS UMR 6097, 06560 Valbonne, France;* [2]*Université de Nice-Sophia Antipolis, 06300 Nice, France;* [3]*Université de Lyon, Centre Européen de Résonance Magnétique Nucléaire à Très Hauts Champs (UMR 5280 CNRS, ENS Lyon, UCBL1), 69100 Villeurbanne, France;* [4]*Pôle Rhône Alpes de Bioinformatique, Université Lyon 1, 69622 Villeurbanne cedex, France;* [5]*Oasi Institute for Research on Mental Retardation and Brain Aging (IRCCS), 94018 Troina, Enna, Italy;* [6]*Institute of Neurological Sciences, National Research Council (ISN-CNR), 95126 Catania, Italy;* [7]*Imperial College London, Biomolecular Medicine, Department of Surgery and Cancer, Faculty of Medicine, South Kensington, London SW7 2AZ, United Kingdom*

Fragile X syndrome (FXS) is the first cause of inherited intellectual disability, due to the silencing of the X-linked Fragile X Mental Retardation 1 gene encoding the RNA-binding protein FMRP. While extensive studies have focused on the cellular and molecular basis of FXS, neither human Fragile X patients nor the mouse model of FXS—the *Fmr1*-null mouse—have been profiled systematically at the metabolic and neurochemical level to provide a complementary perspective on the current, yet scattered, knowledge of FXS. Using proton high-resolution magic angle spinning nuclear magnetic resonance (^{1}H HR-MAS NMR)-based metabolic profiling, we have identified a metabolic signature and biomarkers associated with FXS in various brain regions of *Fmr1*-deficient mice. Our study highlights for the first time that *Fmr1* gene inactivation has profound, albeit coordinated consequences in brain metabolism leading to alterations in: (1) neurotransmitter levels, (2) osmoregulation, (3) energy metabolism, and (4) oxidative stress response. To functionally connect *Fmr1*-deficiency to its metabolic biomarkers, we derived a functional interaction network based on the existing knowledge (literature and databases) and show that the FXS metabolic response is initiated by distinct mRNA targets and proteins interacting with FMRP, and then relayed by numerous regulatory proteins. This novel "integrated metabolome and interactome mapping" (iMIM) approach advantageously unifies novel metabolic findings with previously unrelated knowledge and highlights the contribution of novel cellular pathways to the pathophysiology of FXS. These metabolomic and integrative systems biology strategies will contribute to the development of potential drug targets and novel therapeutic interventions, which will eventually benefit FXS patients.

[Supplemental material is available for this article.]

Fragile X syndrome (FXS) is the most frequent cause of inherited intellectual disability (ID) and the most commonly identified genetic cause of autism (Chelly et al. 2006; Gecz et al. 2009). FXS affects 1 in 4000 males and 1 in 7000 females world-wide (Hagerman 2008) and is caused by the silencing of the X-linked Fragile X Mental Retardation 1 (*FMR1*) gene positioned in Xq27.3. In FXS patients, a dynamic mutation increasing abnormally the number of CGG repeats in the first exon of the *FMR1* gene leads to their hypermethylation and the subsequent absence of its gene product, FMRP (Penagarikano et al. 2007). Although a monogenic disorder, FXS is a disease of complex etiology accompanied by behavioral (hyperactivity, autism), neurological (susceptibility to epileptic seizures), as well as physical abnormalities (macroorchidism, elongated face, hyperextensible finger joints) (Penagarikano et al. 2007). A mouse model of FXS knock-out (KO) for the murine homolog of *FMR1,* has been generated, exhibiting learning and behavioral abnormalities that recapitulate the human phenotype (The Dutch-Belgian Fragile X Consortium 1994). The absence of FMRP induces abnormal extra dendritic spines in neurons of FXS patients and *Fmr1*-KO mice that represent the synaptic defect underpinning the ID (Bassell and Warren 2008; Swanger and Bassell 2011). At the molecular level, FMRP is an RNA-binding protein controlling translation as a component of neuronal messenger ribonucleoprotein (mRNPs) particles associated with somatic and synaptic polyribosomes (Khandjian et al. 2004; Davidovic et al. 2006). FMRP is involved in localized synaptic translation, an essential mechanism that controls protein synthesis locally at the synapse to shape dendritic spines (Bassell and Warren 2008). FMRP and its network of mRNA targets and interacting proteins (Khandjian et al. 2005; Bardoni et al. 2006) contribute to several forms of synaptic plasticity involved in learning and memory processes and notably induced by activation of type I metabotropic glutamate receptors (Dölen and Bear 2008). Although perturbations of these neurospecific events involving FMRP represent the molecular basis of the cognitive impairments observed in FXS patients and *Fmr1*-KO mice, the pathophysiology of FXS remains poorly understood. Since FMRP modulates protein synthesis via direct regulation of the translation of multiple mRNAs, we hypothesize that *Fmr1*-deficiency could functionally affect protein interaction networks with direct consequences on signaling cascades and cellular metabolism.

To investigate this hypothesis, we performed a comprehensive profiling of the metabolome of the *Fmr1*-deficient brain. In order to connect *Fmr1*-deficiency to its metabolic phenotypes, we developed an integrative systems biology approach to map metabolic markers of *Fmr1*-deficiency directly onto the interactome.

[8]**Corresponding authors.**
E-mail davidovic@ipmc.cnrs.fr.
E-mail m.dumas@imperial.ac.uk.
Article published online before print. Article, supplemental material, and publication date are at http://www.genome.org/cgi/doi/10.1101/gr.116764.110.

21:2190–2202 © 2011 by Cold Spring Harbor Laboratory Press; ISSN 1088-9051/11; www.genome.org

Metabonomics is a powerful systems biology approach capturing the variation in low-molecular weight compounds in organs or biofluids in response to pathophysiological interventions or genetic modifications (Nicholson et al. 2002). Metabolic profiling methods, such as proton nuclear magnetic resonance spectroscopy (^{1}H NMR) or mass spectrometry, in conjunction with multivariate pattern recognition analyses, are highly effective in understanding disease processes and drug responses in humans and model organisms (Nicholson et al. 2002), particularly in the case of metabolic diseases (Dumas et al. 2006, 2007). In neuroscience, ^{1}H-NMR metabonomic analysis was used to characterize the neurochemical and metabolic profile of bipolar disorder patients (Lan et al. 2009) and transgenic models of neurological disorders of genetic origin, such as spinal cerebellar ataxia, Huntington's disease, or Batten's disease (Pears et al. 2005; Holmes et al. 2006), as well as Rett Syndrome, the major cause of profound ID in girls (Viola et al. 2007). Hypothesis-free metabolic profiling provides genome-scale metabolic modeling strategies particularly suitable to analyze genotype-phenotype correlations following gene inactivation in animal models of human diseases, in metabolic Quantitative Trait Locus (mQTL) mapping (Dumas et al. 2007) studies or in metabolic genome-wide association studies (Illig et al. 2010). Mapping metabolic biomarkers onto biological networks enhances the understanding of complex metabolic signatures at the pathway level, as typically performed by metabolite-set enrichment analysis (MSEA) (Xia and Wishart 2010; Pontoizeau et al. 2011).

Here we developed a novel alternative strategy which is based on mapping metabolic phenotypes directly onto protein-protein interaction (ppi) networks and analyzing the topology of the resulting network to identify key proteins involved in generating the metabolic phenotype associated in *Fmr1*-deficiency. This novel methodology is particularly suited for studying FXS since *Fmr1*-deficiency directly affects protein networks, and ppi networks are used to unravel the molecular etiology of complex diseases (Navratil et al. 2010, 2011).

In this study, we present the first comprehensive metabolomic profiling of the *Fmr1*-deficient brain in the mouse, using proton high-resolution magic-angle spinning (^{1}H HR-MAS) NMR-based metabonomics, which is particularly suited for small tissue samples analysis. We then define a robust metabolic phenotype (metabotype) of FXS in cerebellum, cortex, striatum, and hippocampus of its mouse model. To understand how *Fmr1*-deficiency mechanistically generates its associated metabolic signature, we present a novel integrative strategy, which we call integrated metabolome and interactome mapping (iMIM), connecting FMRP to its metabolic endpoints via protein-protein interaction networks. Concomitantly, we have used network metrics to identify pivotal proteins or FMRP mRNA targets of the network generating the metabotype associated with *Fmr1*-deficiency and further confirmed their biological relevance in vivo. This novel integrative systems biology strategy highlights the role of key regulatory pathways in FXS pathogenesis, explaining the complexity of the FXS metabotype. In general, iMIM anchors the regulation of complex metabolic phenotypes in protein interaction networks and signaling cascades.

Results

Definition of the optimal spatiotemporal coordinates for metabotyping of the *Fmr1*-deficient brain

We first assessed the patterns of expression of *Fmr1*, the defective gene in FXS, by Western blot and immunohistochemistry to define the optimal spatiotemporal coordinates for metabotyping the developing brain of *Fmr1*-deficient mice (Fig. 1). Western blot analysis of total brain extracts at different post-natal ages reveals that the *Fmr1* gene product, FMRP, is abundantly expressed during the first two post-natal weeks of life, peaking at 5–12 d. Then, FMRP expression strongly decreases as the animal ages to reach lower levels during adulthood (Fig. 1A). These data are consistent with a study reporting a peak of expression of FMRP in the hippocampus and cerebellum during the second post-natal week of life (Lu et al. 2004). To refine the brain regions that express the highest levels of FMRP, we performed immunolabeling on brain sections from 12-d-old wild-type (WT) mice. A strong immunoreactivity was detected in the whole brain (Fig. 1B), particularly in four brain regions: cerebellum, cortex, hippocampus, and striatum (Fig.1C), which manifest dysfunction in FXS patients and *Fmr1*-KO mice (Penagarikano et al. 2007). We, therefore, studied the metabolic consequences of *Fmr1*-deficiency by ^{1}H HR-MAS NMR profiling at this defined post-natal age when FMRP is strongly expressed (Fig. 1). The choice of this specific post-natal age appears also particularly relevant since morphological and physiological defects in the brain of *Fmr1*-KO mice may appear transiently and are often detected in the second post-natal week of life (Nimchinsky et al. 2001; Larson et al. 2005; Bureau et al. 2008; Cruz-Martin et al. 2010), corresponding to the critical time window of active synaptogenesis in the brain. In addition, we restricted our analysis to males to avoid sex-bias in the assessment of FXS metabolic phenotype.

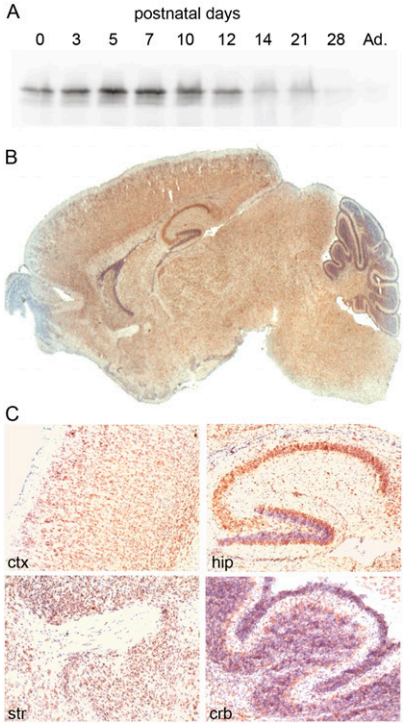

Figure 1. Expression of FMRP in post-natal brain. (*A*) Western blot analysis of FMRP expression in total brain extracts (25 μg/lane) at various post-natal stages and in adult (Ad.). (*B*) Immunohistochemistry on 12-d-old mouse brain longitudinal sections reveal a strong expression of FMRP (brown) in the whole brain and in specific regions (*C*), such as cortex (ctx), hippocampus (hip), striatum (str) and cerebellum (crb). Nuclei were counterstained with cresyl-violet.

Identification of metabolic signature of *Fmr1*-deficiency in mouse brain regions

To derive a metabolic signature associated with FXS, we compared metabolic profiles from intact brain tissues originating from 12-d-old wild-type and *Fmr1*-null male mice ($n = 10$ for each genotype). Compared to classical ^{1}H NMR spectroscopy, generally used to profile liquid tissue extracts, proton high-resolution magic-angle spinning NMR spectroscopy was developed to directly profile intact tissues while preserving cellular integrity—this is particularly suited for characterization of mass-limited samples such as the mouse hippocampus. Supervised multivariate statistical modeling using orthogonal partial least-squares discriminant analysis (OPLS-DA) enables a significant discrimination between *Fmr1*-deficient and control brain regions (Fig. 2). Remarkably, the OPLS-DA three-dimensional (3D) score plot (Fig. 2A) shows that WT brain samples segregate at the periphery of the model, reflecting the anatomical and functional differences between these brain regions also described in the adult rat brain (Tsang et al. 2005). Conversely, *Fmr1*-null mouse brain regions all tend to project toward a common central area in the model. In fact, WT brain regions have a distinct metabolic phenotype whereas *Fmr1*-null brain regions are more alike; this is suggestive of a relatively undifferentiated metabolic state in *Fmr1*-null brains. Interestingly, cortex and cerebellum display remarkably parallel responses to *Fmr1*-deficiency, suggestive of similar metabolic signatures, whereas striatum and hippocampus display unique metabolic signatures (Fig. 3; Table 1). We then compared the respective effects of *Fmr1*-deficiency (KO vs. WT) and of region (ctx vs. crb) on metabolic profiles in an OPLS-based variance components (VC) model (Fig. 2B), showing that the metabolic variation originating from anatomic region (explaining up to 89% of metabolic variation for *myo*-inositol, as measured by the signal at δ3.62) is larger than the genetic variation (up to 36% of ethanolamine variation, δ3.83).

The metabolic signature associated with each brain region is derived from model coefficients obtained from a series of pairwise OPLS-DA models segregating KO from WT for each brain region (Fig. 3) and shows the existence of brain region-specific metabotypes associated with *Fmr1*-deficiency (Table 1). We report here for the first time that, although FMRP is neither an enzyme nor a receptor directly involved in neurotransmitter metabolism or signaling, *Fmr1*-deficiency has dramatic impacts on the levels of six neurotransmitters (gamma-amino butyric acid [GABA], glutamate, acetylcholine [Ach], taurine, alanine, and aspartate) and several of their precursors or catabolites (glutamine, acetate, choline, and *N*-acetyl aspartate [NAA]) (Table 1). The *Fmr1*-deficient metabotypes also involve the osmolyte and the secondary messengers precursor *myo*-inositol, intermediary metabolites and lipids totally unrelated to neurotransmission (acetoacetate, lactate and carbonyls from fatty acids). At the network level, 25 metabolites undergo significant alterations in the *Fmr1*-null brain (Table 1) and may be considered as global FXS biomarkers.

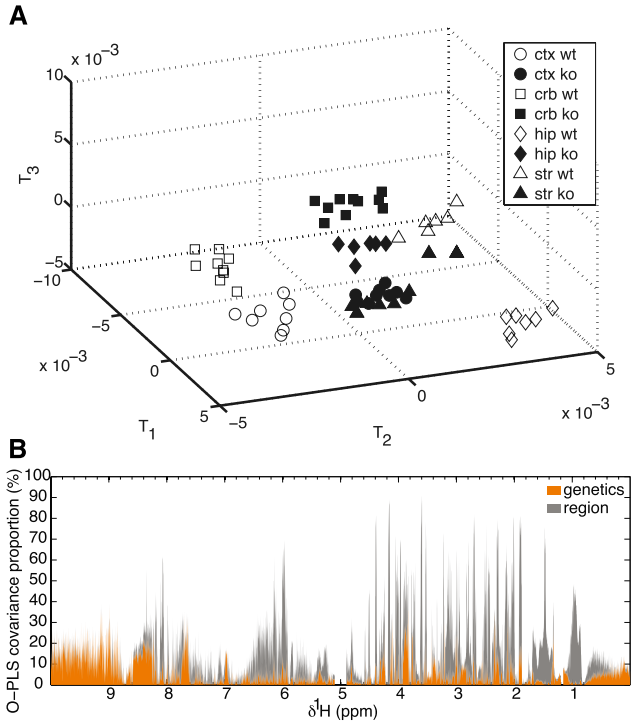

Figure 2. Metabolic signature of *Fmr1*-deficiency in 12-d-old brain. The metabolic variation observed in ^{1}H NMR spectra acquired in 12-d-old mouse brain samples was modeled using an orthogonal partial least square-discrimination analysis (OPLS-DA). PLS components maximizing the segregation of the groups are computed. Each PLS component corresponds to a combination of the initial ^{1}H NMR spectral variables, known as model coefficients or loadings. Each individual spectrum has new coordinates on the PLS components, known as scores. As a consequence, the three-dimensional OPLS-DA scores plot (*A*) segregates the different sample groups according to brain region (shapes) and *Fmr1*-deficiency status (white and black shapes). (*B*) OPLS variance component model of cortex and cerebellum. (Ctx) cortex, (crb) cerebellum, (hip) hippocampus, (str) striatum, (ko) *Fmr1*-knockout, (wt) wild-type samples.

Metabolite Set Enrichment Analysis (MSEA) of *Fmr1*-deficiency metabotypes

A Metabolite-Set Enrichment Analysis (MSEA) (Xia and Wishart 2010), an extension of the Gene Set Enrichment Analysis (GSEA) (Subramanian et al. 2005), was then used to test for metabolic pathways enrichment in each brain region. In the cortex, *Fmr1*-deficiency is significantly associated with: an increase in lipid-oxidized species (mainly carbonyls, such as CH_3-$\underline{CH_2}$-CH_2-CO- and -$\underline{CH_2}$-CO-) and acetoacetate, and a decrease in GABA and glutamate, their precursor, glutamine, as well as in *N*-acetyl-aspartate (NAA) and lactate (Table 1). The decreased cortical levels of glutamine corroborate a previous study using reversed-phase high-performance liquid chromatography (HPLC) (Gruss and Braun 2001) on *Fmr1*-KO and WT cortex, and we confirmed, using an enzymatic assay, that the cortical levels of glutamate were significantly decreased in *Fmr1*-KO animals ($P = 0.011$) (Fig. 4A). In addition, the increase in carbonyl groups that we observe in the cortex was previously documented using a biochemical approach (El Bekay et al. 2007). These data strongly support the robustness of ^{1}H HR-MAS NMR to identify metabolic changes in *Fmr1*-deficient brain. Subsequent MSEA analysis (Xia and Wishart 2010) highlights that significant cortical alterations in glutamine/glutamate metabolism, in synthesis and degradation of ketone bodies, as well as in glutathione metabolism derive from this metabotype (Supplemental Table S1). In the cerebellum, decreases in glutamine, GABA, NAA, *myo*-inositol (whereas its stereoisomer *scyllo*-inositol is increased), aspartate, and acetate associated with increases in both Ach and its precursor, choline (Table 1), correlate with significant alteration in glycerophospholipid and β-alanine metabolism (Supplemental Table S1). Interestingly, the reduced glutamine levels in *Fmr1*-deficient cerebellum were also detected by others (Gruss and Braun 2001), and we have been able to confirm by

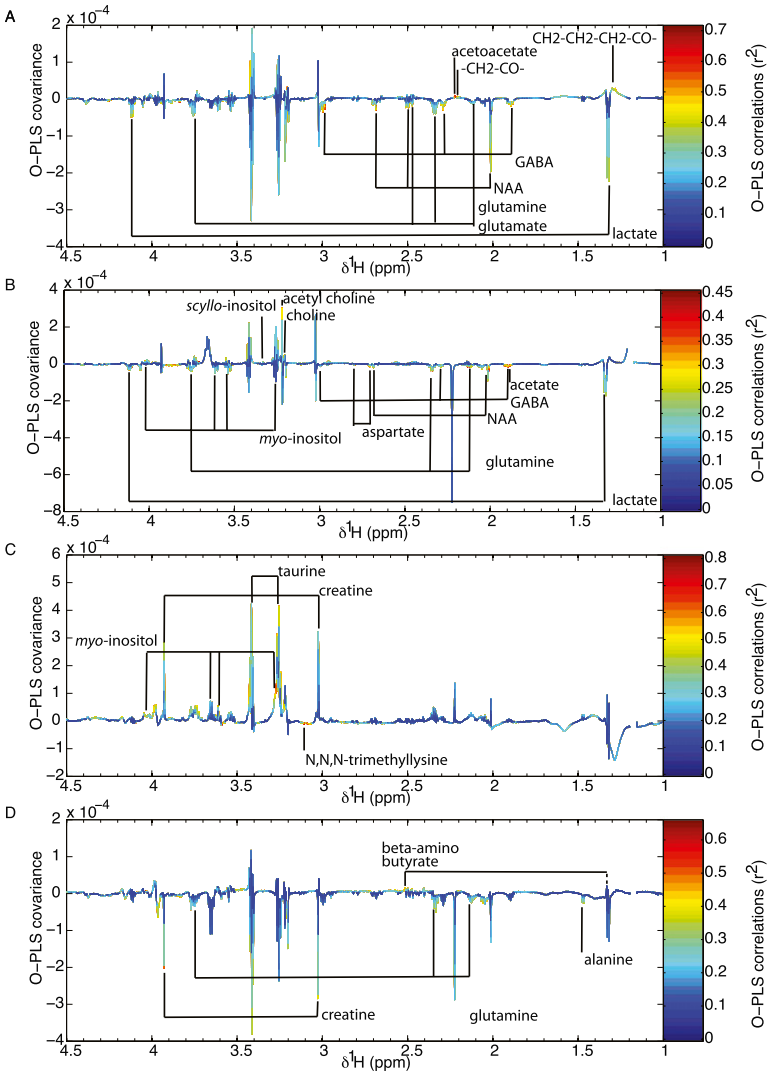

Figure 3. Region-specific metabolic signature of *Fmr1*-deficiency in 12-d-old brain. Metabolic variations in ^{1}H NMR spectra obtained from *Fmr1*-null and wild-type mice were assessed independently for each brain region by OPLS-DA. These OPLS-DA models are represented as a pseudo-spectrum. Positive model coefficients correspond to higher metabolite concentrations in KO animals, whereas negative model coefficients are associated with higher metabolite concentrations in WT animals. Metabolic signature as obtained from cortex (Q^2Y_{hat} = 0.61) (*A*), cerebellum (Q^2Y_{hat} = 0.57) (*B*), hippocampus (Q^2Y_{hat} = 0.84) (*C*), and striatum (Q^2Y_{hat} = 0.44) (*D*).

ELISA a significant decrease in GABA cerebellar concentrations in *Fmr1*-KO animals (P = 0.038) (Fig. 4B). The hippocampus displays increases in taurine, creatine, and *myo*-inositol that evoke alterations in taurine/hypotaurine metabolism and inositol phosphate metabolism (Table 1; Supplemental Table S1). Of particular interest, increased taurine levels were also reported in hippocampus of *Fmr1*-KO animals by a previous study (Gruss and Braun 2001). Finally, in the striatum, a decrease in kynurenine (Table 1) drives significant alterations of tryptophan metabolism (Supplemental Table S1), coupled to decreases in alanine, creatine, and adenine.

Integrated metabolome and interactome mapping of *FMRI*-deficiency metabotypes

To bring a mechanistic understanding in our genotype-phenotype associations and functionally connect the causal mutation in the *FMR1* gene with the downstream metabolic biomarkers derived from the OPLS-DA models presented above, we developed a novel network biology strategy—integrated metabolome and interactome mapping. Databases and literature data sets were gathered to reconstruct a molecular interaction network (see Supplemental Table S2 for an exhaustive list of sources, and see Methods for detailed construction of the interactome) encapsulating (1) known and putative mRNAs regulated by FMRP resulting from either large-scale screenings or individual characterization of direct RNA-protein interactions, (2) the known FMRP protein-protein interactome, including kinases, and (3) metabolic (KEGG database) (Kanehisa et al. 2008) and neuronal signaling pathways (NeuronDB, Yale University). Since our iMIM approach uses databases with human annotations, we chose to standardize and use the official human gene and protein symbols in the related paragraphs, even though proteins or mRNA interactors might have been identified in a variety of organisms. The topology of the resulting integrated metabolome interactome mapping network was then analyzed to visualize functional paths between FMRP and its associated metabotypes and to model how inactivation of *FMR1* propagates through the cellular network until it reaches its metabolic endpoints (Fig. 5A). Considering a given metabolite M and using the Ockham's razor principle, the shortest path between FMRP and M through the interactome network is likely to provide a mechanistic link between *FMR1*-deficiency and its consequence on metabolite M. Since FMRP is neither an enzyme nor a receptor, the shortest path between FMRP and M becomes: FMRP → interacting protein or mRNA-target → enzyme (or receptor) → metabolite M, where the shortest path length (spl) is 3. The spl becomes 2 in the case of a receptor or enzyme being an interacting protein or mRNA target. The average spl computed from the entire knowledge network between FMRP and the 25 metabolites identified as FXS markers by NMR is 3.38, which approaches 3, meaning that FMRP is connected to a perturbed metabolite via one of its mRNA targets or protein partners, which in turn will interact with a receptor or enzyme. This spl is significantly lower than the average spl obtained from randomly resampled lists of 25 biomarkers with 100,000 H_0 iterations (spl = 3.38, P = 0.03427) (Fig. 5B), which confirms that *FMR1*-deficiency is selectively connected to the perturbed metabolites identified above.

Centrality-based stratification of proteins in the iMIM network using pivotal betweenness

Based on the iMIM network and the set of all shortest paths, we then assessed the centrality of a given protein or mRNA-target

Table 1. Metabolic signature of *Fmr1*-deficiency

Fmr1-KO metabotypes	Brain region				Component	
	ctx	crb	hip	str	Genetic	Region
Lactate	↓	↓			↓	
Glutamine	↓	↓			↓	
GABA[a]	↓	↓			↓	↑
N-acetyl-aspartate	↓	↓			↓	↓
Glutamate[a]	↓				↓	
Acetotacetate	↑					
$C\underline{H}_2$-CO	↑					
$C\underline{H}_2$-CH_2-CH_2-CO	↑					
Myo-inositol		↓	↑			
Aspartate[a]		↓				
Acetate		↓			↓	
Acetylcholine[a]		↑				↑
Choline		↑				↑
Scyllo-inositol		↑				
N,N,N trimethyl lysine			↓			
Taurine[a]			↑		↑	
Creatine			↑	↓		
Alanine[a]				↓		↓
Beta-amino butyrate				↑		
Kynurenine				↓		
N-alpha acetylornithine				↓		
Adenine				↓		
Inosine					↑	
Purine					↑	↑
Ethanolamine					↓	

Metabotypes derived from Figures 2 and 3 are summarized for each model, by brain regions (OPLS-DA models) (Fig. 3) or by using variance components (factors: genetic or region) (Fig. 2B). (Ctx) cortex, (crb) cerebellum, (hip) hippocampus, (str) striatum.
[a]Neurotransmitters.

between *FMR1*-deficiency and its metabolic endpoints by estimating their pivotal betweenness (PB). PB is a measure of centrality, meaning that graph edges used by several shortest paths will have a high PB (see Methods; Table 2; Supplemental Table S3). This continuous variable is directly correlated to the weight of the proteins in the shortest paths of the network and enables a systematic stratification and ranking of these proteins based on their relative importance at the network scale. The iMIM network derived from the metabolic signature of FXS highlights that among the 30 most pivotal proteins, 13 are either FMRP protein interactors, such as the protein FXR2P (PB = 8.23×10^{-6}) (Zhang et al. 1995), the homolog of FMRP, or are encoded by mRNA targets of FMRP (Fig. 5), such as the mRNA encoding super oxide dismutase 1 (SOD1, PB = 1.35×10^{-5}) (Bechara et al. 2009), amyloid beta precursor protein (APP, PB = 1.56×10^{-5}) (Westmark and Malter 2007), calcium/calmodulin-dependent protein kinase II alpha (CAMK2A, PB = 7.93×10^{-6}) (Iacoangeli et al. 2008), eukaryotic translation elongation factor 1 alpha 1 (EEF1A1, PB = 6.06×10^{-6}) (Sung et al. 2003), and microtubule-associated protein 1B (MAP1B, PB = 3.93×10^{-6}) (Brown et al. 2001; Chen et al. 2003; Lu et al. 2004; Iacoangeli et al. 2008). Interestingly, poorly characterized putative mRNA FMRP targets, such as the mRNA encoding the small GTP-ase and cytoskeleton-regulator RHOA (PB = 1.83×10^{-5}) (Chen et al. 2003) and the calcium regulatory protein Calbindin1 (CALB1, PB = 1.35×10^{-5}) (Miyashiro et al. 2003), appear as pivotal in our network (Table 2; Fig. 5); RHOA connects FMRP to four of the perturbed metabolites, while CALB1 relays FMRP to metabolic perturbations of the osmolyte and secondary messenger *myo*-inositol (Fig. 5).

Biological confirmation of the in vivo association of FMRP with mRNA encoding pivotal proteins of the iMIM network

The pivotal FMRP mRNA targets highlighted in silico by the iMIM network were initially identified in large-scale screenings for FMRP mRNA targets, and some still lack extensive biological validation. We, therefore, sought to further confirm that FMRP physically interacts with iMIM-derived pivotal mRNA targets in vivo (Fig. 5A), using UV-crosslinking and immunoprecipitation assays (CLIP) (Ule et al. 2005). Compared to classical immunoprecipitation, the CLIP approach uses UV-crosslinking irradiation of tissues to generate covalent bonds between nucleic acids and proteins, thereby preserving the labile interaction between mRNA and proteins that are often lost in classical immunoprecipitation. Immunoprecipitation of FMRP mRNA complexes was carried out using the R60 polyclonal antibody raised against the C terminus of FMRP on *Fmr1*-WT and KO total P12 brain extracts (See Supplemental Fig. S1 for exhaustive characterization of the R60 antibody). As expected, FMRP was not detected in input or immunoprecipitate from *Fmr1*-KO animals, whereas it was recovered in WT input and immunoprecipitate (Fig. 6A). In addition, two known interactors of FMRP, its homologues FXR1P and FXR2P (Zhang et al. 1995), present in equal levels in the *Fmr1*-KO and WT input, are only recovered in the WT immunoprecipitate (Fig. 6A), confirming the specificity of the immunoprecipitation. RT-PCR analysis of mRNAs extracted from *Fmr1*-WT and KO input and immunoprecipitates was then carried out (Fig. 6B). The equal intensity of the bands corresponding to the studied mRNAs reveal that *Mtap1b*, *Tubb3*, *Sod1*, *Rhoa*, and *Calb1* mRNAs are expressed at similar levels in the input fraction from *Fmr1*-KO and WT brain (Fig. 6B). *Fmr1* mRNA was detected in WT input and immunoprecipitate (Fig. 6B, lanes 2,4), together with the known mRNA target of FMRP encoding

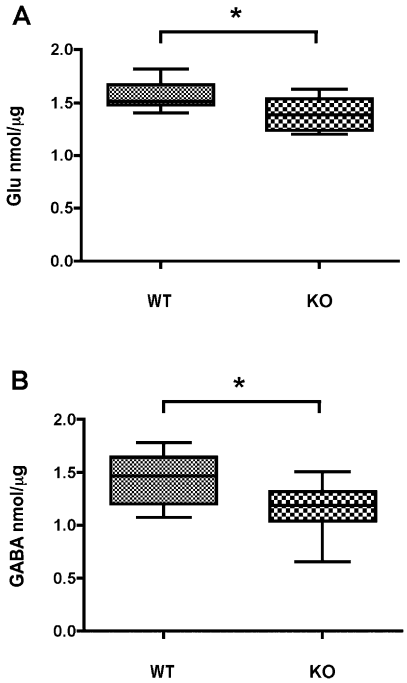

Figure 4. Quantification of glutamate levels in cortical extracts and GABA levels in cerebellar extracts of *Fmr1*-KO brain vs. WT. Glutamate cortical (*A*) and GABA cerebellar concentrations (*B*) are significantly reduced in *Fmr1*-KO extracts compared to WT ($P = 0.011$; $P = 0.038$, respectively; $n = 9$ for each genotype).

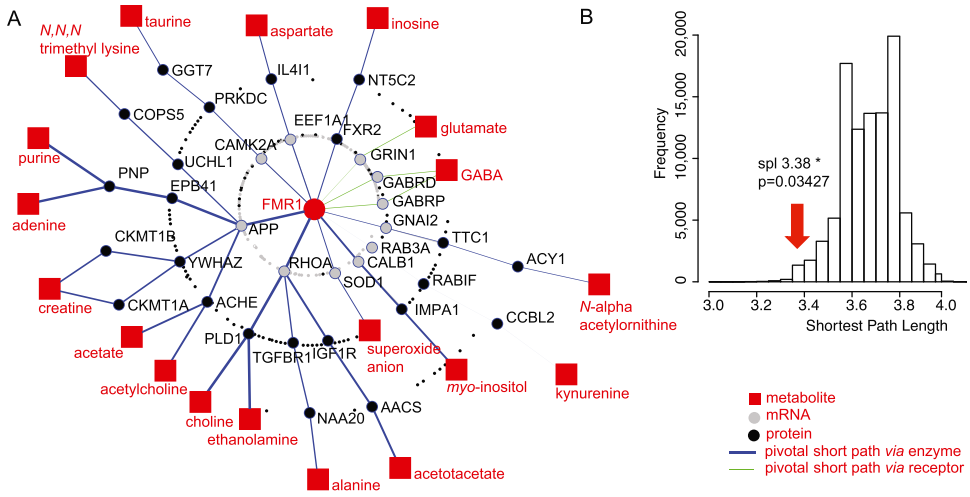

Figure 5. Interactome-mapping of *FMR1*-deficiency metabotype. (*A*) *FMR1* integrated metabolome and interactome mapping (iMIM) network. The metabolites significantly affected in the different models (Table 1) were mapped onto the interactome, using FMRP mRNA targets and protein interactors, KEGG metabolic pathways, and neurotransmitter/receptor databases. The resulting network allows connecting of the causal gene *FMR1* to the downstream metabolic consequences of its deficiency. Pivotal shortest paths via enzymes and receptors are represented in blue and green, respectively. (*B*) Statistical validation of the *FMR1* knowledge network under the null hypothesis (H_0). The average shortest path length (spl) between *FMR1* and the biomarker metabolites ($n = 25$) was computed and compared to the distribution of average spl obtained after 100,000 H_0 network simulations (i.e., networks obtained after 100,000 random selections of 25 metabolites from the entire metabolic network). This simulation under the null hypothesis shows that *FMR1* appears significantly connected to the candidate biomarker metabolites, with an average distance of 3.38 hops ($n = 100{,}000$ random simulations, $P = 0.03427$).

microtubule-associated protein 1B, *Mtap1b* (Fig. 6A, lane 4), corroborating previous studies (Lu et al. 2004; Iacoangeli et al. 2008). Conversely, no amplicon corresponding to the unrelated mRNA encoding beta-Tubulin 3 (*Tubb3*) was detected in either immunoprecipitate. Similar results were obtained with another negative control—the mRNA encoding phosphoglycerate kinase 1 (*Pgk1*, not shown)—thereby confirming the specificity of the approach. Interestingly, the mRNA *Sod1* was detected in the WT immunoprecipitate (Fig. 6B, lane 4), showing for the first time its in vivo association with FMRP in brain. Also, the mRNA *Rhoa* and *Calb1* encoding pivotal proteins of the network were also specifically recovered in the *Fmr1*-WT immunoprecipitates (Fig. 6B, lane 4). Altogether, these data confirm the association of FMRP with *Rhoa* and *Calb1* mRNAs suggested by high-throughput screening and strongly support the fact that these mRNAs are in vivo targets of FMRP.

Identification of perturbed pathways in *Fmr1*-deficient brain

Further GSEAs (Subramanian et al. 2005) were carried out on the iMIM network's pivotal proteins to identify significantly perturbed pathways in *Fmr1*-null mouse brain. GSEA was performed by comparing Gene Ontology (Rivals et al. 2007) (Supplemental Table S4) and KEGG (Kanehisa et al. 2008) (Supplemental Table S5) annotations of the pivotal proteins ($n = 257$) to those of the entire set of proteins present in the iMIM network. Typical enriched terms from GSEA show that the metabolic signature of the FXS mouse model translates into perturbations of "central nervous system development," "signaling," and "function and metabolism," among which were alterations of "glutamate signaling pathways," "protein kinase cascade," "actin cytoskeleton organization and biogenesis," and "synaptic transmission" coupled to "behavior and learning and memory defects."

Discussion

Although FXS is a monogenic disorder, *Fmr1*-deficiency genotype/phenotype associations are difficult to assess from a mechanistic point of view, since FMRP is involved in the translation of numerous mRNAs and affects the levels of proteins involved in a wide range of cellular processes (Darnell et al. 2005). This conceptual difficulty required the development of a novel integrative systems biology method to mechanistically understand the metabolic consequences of *Fmr1*-deficiency. In this study, we profiled the metabolome of the brain of the mouse model of FXS using ^{1}H HR-MAS NMR spectroscopy, to gain knowledge on FXS metabolism. We then developed the integrated metabolome and interactome mapping framework and its associated network metric, the pivotal betweenness. This strategy allowed us to get new insight into FXS pathophysiology and to identify key FMRP mRNA targets involved in regulating its metabolic phenotype, as discussed in detail below.

Comprehensive metabolic profiling of the brain of the mouse model of FXS: Identification of *Fmr1*-deficiency metabolic phenotypes specific to each brain region

Using ^{1}H HR-MAS NMR spectroscopy-based metabolic profiling, we show that the absence of FMRP affects the metabolic phenotype of the developing brain in a region-specific manner, with cortex and cerebellum being the most affected regions. In the wild type, each brain region has a unique metabolic profile, which translates into a clustering of the samples according to brain region in the OPLS-DA 3D scores plot (Fig. 2A). This is suggestive of region-specific functions and metabolisms even at this early postnatal age and corroborates a previous metabolomic study on adult rat brain (Tsang et al. 2005). This clustering becomes considerably less evident in the *Fmr1*-deficient brain, where samples are projected toward the center of the model in a more homogenous manner. The incomplete metabolic differentiation observed in the *Fmr1*-deficient brain might be related to the general delayed maturation of the *Fmr1*-KO brain suggested by the immature-looking dendritic spines in Fragile X mice and human patients (Nimchinsky et al. 2001; Larson et al. 2005; Bureau et al. 2008; Cruz-Martin et al. 2010), but it is also directly linked to the functional consequences

Table 2. Top 30 pivotal proteins derived from interactome mapping of *Fmr1*-deficiency metabotypes

Rank	Human gene accession number	Official protein symbol	Full protein name	Reference	Pivotal betweenness
1	ENSG00000067560	RHOA[a]	Ras homolog gene family, member A	(Chen et al. 2003)	1.83×10^{-5} *
2	ENSG00000075651	PLD1	Phospholipase D1, phosphatidylcholine-specific		1.79×10^{-5} *
3	ENSG00000198805	PNP	Purine nucleoside phosphorylase		1.59×10^{-5} *
4	ENSG00000142192	APP[a]	Amyloid beta (A4) precursor protein	(Westmark and Malter 2007)	1.56×10^{-5} *
5	ENSG00000142168	SOD1[a]	Superoxide dismutase 1, soluble	(Bechara et al. 2009)	1.35×10^{-5} *
6	ENSG00000104327	CALB1[a]	Calbindin 1, 28 kDa	(Miyashiro et al. 2003)	1.35×10^{-5} *
7	ENSG00000133731	IMPA1	Inositol(myo)-1(or 4)-monophosphatase 1		1.35×10^{-5} *
8	ENSG00000087085	ACHE	Acetylcholinesterase		1.12×10^{-5} *
9	ENSG00000129245	FXR2[a]	Fragile X mental retardation, autosomal homolog 2	(Zhang et al. 1995)	8.23×10^{-6} *
10	ENSG00000070808	CAMK2A[a]	Calcium/calmodulin-dependent protein kinase II alpha	(Iacoangeli et al. 2008)	7.93×10^{-6} *
11	ENSG00000070748	CHAT	Choline *O*-acetyltransferase		7.86×10^{-6} *
12	ENSG00000113580	NR3C1[a]	Glucocorticoid receptor, group C, member 1	(Miyashiro et al. 2003)	7.45×10^{-6} *
13	ENSG00000094755	GABRP[a]	Gamma-aminobutyric acid (GABA) A receptor, pi	(Miyashiro et al. 2003)	6.73×10^{-6} *
14	ENSG00000187730	GABRD[a]	Gamma-aminobutyric acid (GABA) A receptor, delta	(Miyashiro et al. 2003)	6.73×10^{-6} *
15	ENSG00000076685	NT5C2	5′-nucleotidase, cytosolic II		6.73×10^{-6} *
16	ENSG00000196839	ADA	Adenosine deaminase		6.73×10^{-6} *
17	ENSG00000156508	EEF1A1[a]	Eukaryotic translation elongation factor 1 alpha 1	(Sung et al. 2003)	6.06×10^{-6}
18	ENSG00000081760	AACS	Acetoacetyl-CoA synthetase		5.64×10^{-6}
19	ENSG00000114353	GNAI2[a]	Guanine nucleotide binding protein, alpha inhibiting activity polypeptide 2	(Miyashiro et al. 2003)	4.88×10^{-6}
20	ENSG00000104951	IL4I1	Interleukin 4 induced 1		4.49×10^{-6}
21	ENSG00000104951	AKT1S1	AKT1 substrate 1 (proline-rich)		4.49×10^{-6}
22	ENSG00000104951	NUP62	Nucleoporin 62 kDa		4.49×10^{-6}
23	ENSG00000128050	PAICS	Phosphoribosylaminoimidazole carboxylase		4.49×10^{-6}
24	ENSG00000140443	IGF1R	Insulin-like growth factor 1 receptor		4.37×10^{-6}
25	ENSG00000198931	APRT	Adenine phosphoribosyltransferase		4.35×10^{-6}
26	ENSG00000171105	INSR	Insulin receptor		4.19×10^{-6}
27	ENSG00000118689	FOXO3[a]	Forkhead box O3	(Brown et al. 2001)	4.11×10^{-6}
28	ENSG00000131711	MAP1B[a]	Microtubule-associated protein 1B	(Brown et al. 2001; Darnell et al. 2001; Chen et al. 2003)	3.92×10^{-6}
29	ENSG00000131067	GGT7	Gamma-glutamyltransferase *7*		3.78×10^{-6}
30	ENSG00000141510	TP53	Tumor protein p53		3.43×10^{-6}

Proteins involved in the interaction network (Fig. 5) were ranked by pivotal betweenness (PB). Accession numbers for the genes encoding these pivotal proteins are provided in the table. Asterisks indicate PB values that appear in the 5% quantile of the PB values distribution.
[a]Proteins directly interacting with FMRP or encoded by FMRP mRNA targets; corresponding reference provided in brackets.

of the absence of FMRP and the interactions with its mRNA targets and protein partners. However, the events leading to this spine dysgenesis in FXS appear to be a complex mix of abnormal nervous system early development (Callan and Zarnescu 2011), delayed maturation (Bureau et al. 2008; Cruz-Martin et al. 2010), and altered stabilization and pruning (Swanger and Bassell 2011), FMRP being involved in each of these processes via regulation of its mRNA targets and protein partners. This illustrates that the observed delayed maturation of the *Fmr1*-deficient brain and the lack of *Fmr1* function cannot be completely disentangled. This prompted us to use novel integrative systems biology approaches to explore the functional consequences of *Fmr1*-deficiency on metabolism.

Identification of metabolic pathways perturbed by *Fmr1*-deficiency

To investigate how *Fmr1*-deficiency results in the metabotypes that we detected in the brain of the mouse model of FXS, we first applied a recent integrative systems biology strategy, testing which metabolic pathways are significantly affected—metabolite-set enrichment analysis (MSEA) (Xia and Wishart 2010; Pontoizeau et al. 2011; Supplemental Table S1). This analysis contributed to the identification of the principal metabolic pathways perturbed in the brain of the mouse model of FXS.

Fmr1–deficiency drives alterations in neurotransmitters levels

Our results show that FXS brain undergoes global alterations in neurotransmitter metabolism, mainly glutamate, GABA, acetylcholine, and taurine. In the *Fmr1*-deficient cortex, the reduction of glutamine and glutamate metabolism we observe might result in a reduction of the amounts of released glutamate, with important consequences on the functioning of cortical circuitry and cortical excitability, as previously reported (Gibson et al. 2008). In *Fmr1*-deficient mice, the reduced mRNA levels of *Gad1*, encoding the glutamate-decarboxylase Gad65 that catalyzes the conversion of glutamate into GABA (D'Hulst et al. 2009) (Fig. 7), may explain the decreased cortical and cerebellar GABA levels. Given the essential role of GABA for the development of cortex and cerebellum, lower GABA levels might perturb optimal development of these structures, especially at 11–12 d old, a stage which encompasses the time window when GABA shifts from excitatory toward inhibitory effects, as reported in rat (Ben-Ari et al. 2007). On the other hand, our data suggest that the *Fmr1*-deficient hippocampus undergoes increased neuronal inhibition mediated by taurine during early post-natal development (El Idrissi and Trenkner 2004). Finally, a decrease in acetylcholine and its precursor, choline, suggests a disruption of the cholinergic system in the *Fmr1*-deficient cerebellum (Fig. 7), which plays an essential developmental role in this region (De Filippi et al. 2005). In conclusion, the delicate balance between excitatory and inhibitory inputs appears compromised

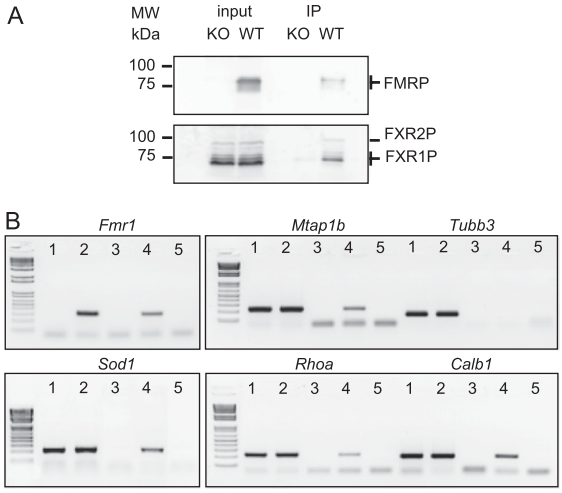

Figure 6. *Fmr1*, *Mtap1b*, *Sod1*, *Rhoa*, and *Calb1* mRNAs interact with FMRP in vivo. (*A*) Western blot analysis of UV-crosslinking and immunoprecipitation (CLIP) assay performed on *Fmr1* wild-type (WT) and knockout (KO) total brain lysates using polyclonal antibodies raised against the C terminus of FMRP. Input lysate (1/100th) and immunoprecipitates (IP, 1/20th) were probed for FMRP and its interacting protein partners FXR1P and FXR2P, respectively, by western blotting, revealing the presence of FMRP in the WT immunoprecipitates (*upper* panel revealed with 1C3 antibody), together with interacting partners FXR1P and FXR2P (lower panel revealed by 3Fx antibody). (*B*) RT-PCR analysis of mRNAs associated with FMRP. Total RNA was extracted from the input brain lysate and immunoprecipitates described in *A*, and used as a template for RT-PCR. RT-PCR products obtained from *Fmr1*-KO (lane *1*) and WT (lane *2*) inputs and from immunoprecipitates of *Fmr1*-KO (lane *3*) and WT (lane *4*) brain extracts were separated and visualized by agarose gel electrophoresis. This reveals that the known FMRP mRNA targets *Fmr1* and *Mtap1B* are selectively recovered in the WT immunoprecipitate, while the unrelated mRNA *Tubb3* is not recovered. *Sod1* mRNA is also selectively recovered in the immunoprecipitate together with *Rhoa* and *Calb1* mRNAs. Control PCR (lane *5*) was performed in the absence of reverse-transcriptase. Lower DNA molecular weight markers presented on the *left* of the gels are, respectively, 100, 200, 300, 400, 500, 600, 800, and 1000 bp.

in the mouse model of FXS at this early post-natal stage corresponding to the time-window of synaptogenesis, with direct consequences on neuronal circuits formation development (Akerman and Cline 2007).

Altered osmolyte and secondary messengers balance

In the *Fmr1*-deficient brain, we observed variations in osmolytes such as NAA, *myo*-inositol, and taurine. Osmolytes control the ion gradient across membranes, and modifications of their levels may facilitate neuronal discharge and epileptiform activity (Liu et al. 2008), as described in the *Fmr1*-deficient mouse (Qiu et al. 2008). In addition, disruption of osmolyte balance is widely observed in various neurological conditions, and constitutes a hallmark of brain dysfunctions (Pears et al. 2005; Viola et al. 2007; Lan et al. 2009). Alternatively, decreased *myo*-inositol levels in the hippocampus and increased levels in the cerebellum of *Fmr1*-deficient mice suggest dysregulations of phosphoinositide metabolism since *myo*-inositol is a precursor for these important secondary messengers. Our findings support the idea that *Fmr1*-deficiency might modify neuronal physiology in a nonspecific manner, through osmoregulation and secondary messenger signaling machinery.

Disruption of post–natal energy metabolism and neuron/glia metabolic cooperation in the FXS brain

Astrocytes and neurons cooperate metabolically for neuronal energy fueling and biosynthesis of neurotransmitters (Fig. 7). In the *Fmr1*-deficient brain, the decreased levels of lactate in cerebellum and cortex and the increase in the ketone-body acetoacetate in cerebellum might reflect a disruption of neuronal metabolic fueling during post-natal brain development. These metabolites are the essential source of neuronal energy, thus replacing glucose at this specific period to replenish acetyl-coA stores to fuel the tricarboxylic acids (TCA) cycle (Pellerin 2008) (Fig. 7). Glutamate and GABA can also enter the TCA cycle via conversion upstream or downstream via the intermediate metabolite alpha-ketoglutarate (αKG) (Fig. 7). Altered glutamine, glutamate, and GABA levels also support a disruption of the interplay between glia and neurons controlling the glutamine–glutamate–GABA cycle (McKenna 2007) (Fig. 7). Our results highlight the readjustment of TCA cycle and energy metabolism in neurons and glial cells in the absence of FMRP.

Adaptative response to increased oxidative stress

We have identified a marked increase in cortical oxidative stress markers, such as lipid peroxidation products, notably aldehydes and carbonyls species. These species result from free radical attack of unsaturated lipids by superoxide anions, normally detoxified by SOD1. We previously observed this specific metabotype in *sod1*-deficient *Caenorhabditis elegans* (Blaise et al. 2007). Interestingly, we have shown that FMRP binds in vitro *Sod1* mRNA and that its absence decreases the cortical levels of SOD1 (Bechara et al. 2009), a pivotal protein in our network (Table 2; Figs. 5, 6). Here, we have shown the association of FMRP with *Sod1* mRNA in vivo (Fig. 6B). These data directly correlate depletion of SOD1 to biochemical and enzymatic markers of enhanced oxidative stress in the brains of *Fmr1*-deficient mice (increase in carbonyl groups in the cortex (El Bekay et al. 2007; this study). These data indicate that increased oxidative stress is a phenotypic trait of FXS.

Development of the iMIM framework and associated network metrics to identify key FMRP targets involved in regulating its metabolic phenotype

iMIM and pivotal betweenness

FMRP is a translational regulator and has no direct link with metabolism, apart from SOD1. However, it interferes with protein-protein interaction networks via regulation of the levels of the proteins encoded by its mRNA targets. To investigate the *Fmr1*-deficiency metabolic phenotype/genotype association, we developed a new approach, which we called integrated metabolome and interactome mapping. In iMIM, the metabolic markers associated with *Fmr1*-deficiency were mapped onto metabolic pathways and protein-protein interaction networks (Fig. 5; Table 2). Close analysis by GSEA of the most significantly enriched biological functions in the resulting network shows that the metabolic perturbations in the brains of *Fmr1*-deficient mice are associated with various biological processes typically related to CNS and neuron development, cognitive functions, signal transduction, and neurotransmitter metabolism (Supplemental Tables S4, S5). To identify the key proteins related to these processes that may link *Fmr1*-deficiency consequences to metabolism, we analyzed the network topology by estimating the pivotal betweenness of

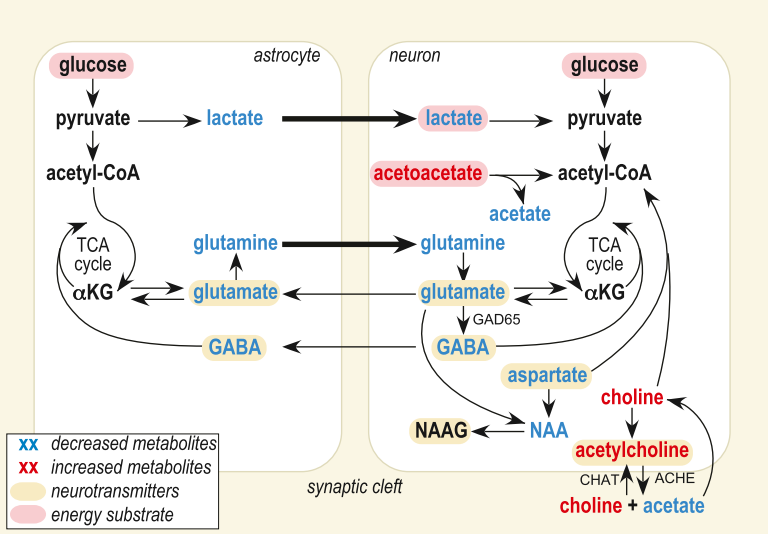

Figure 7. Schematic metabolic map of *Fmr1*-deficiency in cortex and cerebellum. Astrocytes and neurons cooperate metabolically for neuronal energy fueling and biosynthesis of neurotransmitters, and this cooperation seems compromised in the *Fmr1*-null brain. Glucose, lactate, and acetoacetate are neuronal energy substrates (framed in pink) which contribute to replenish acetyl-coA stores to fuel the tricarboxylic acid cycle. Glutamate and GABA can enter the TCA cycle via conversion upstream of or downstream from the intermediate metabolite alpha-ketoglutarate (αKG). Metabolites affected by *Fmr1*-deficiency are represented in blue if decreased and red if increased. Metabolites acting as neurotransmitters are represented in yellow frames. (NAA) *N*-acetyl-aspartate, (NAAG) *N*-acetyl-aspartyl-glutamate, (GAD65) glutamate dehydrogenase, (CHAT) choline *O*-acetyltransferase, (ACHE) acetylcholinesterase.

each protein of the network. We defined this network metric to enable a systematic stratification and ranking of the proteins based on their relative importance at the network scale (Fig. 5; Table 2; Supplemental Tables S3, S4). Among the 30 pivotal proteins of the network, 13 are encoded by putative or confirmed mRNA targets of FMRP. To confirm the biological relevance of the identified key regulatory proteins, we validated in vivo the association of FMRP in brain with their corresponding mRNA, notably *Sod1*, *Rhoa*, and *Calb1* (Fig. 6B), thereby ascertaining the robustness of our approach.

Identification of key FMRP mRNA targets and proteins and pathways involved in FXS

The two principal branches of the network involve two proteins encoded by the confirmed mRNA target of FMRP *APP* (Westmark and Malter 2007), and an mRNA target we confirmed in vivo, *Rhoa* (Chen et al. 2003; Fig. 6B), which, respectively, regulate six and four metabolites. APP plays a central role in synaptic functions and Alzheimer's disease (Kamenetz et al. 2003), and genetic dysregulations of the cytoskeleton-regulators *RHOA* family are linked to ID (Benarroch 2007). These data suggest that alterations of the levels of RHOA and APP proteins in the absence of FMRP may have direct neuronal consequences. Interestingly, APP and RHOA interact with two important enzymes in our iMIM network (Fig. 5; Table 2) involved in acetylcholine metabolism: respectively, acetylcholine esterase (ACHE) (Fig. 7; Cottingham et al. 2002), the enzyme degrading Ach into acetate and choline, and phospholipase D1 (PLD1) (Fig. 7; Klein 2005), which provides free choline for the synthesis of Ach in the brain. Our iMIM analysis also reveals that another key enzyme involved in acetylcholine metabolism [choline *O*-acetyltransferase (CHAT)] is pivotal (Figs. 3, 7; Table 2). These data support the involvement of the cholinergic system in FXS, suggested by the fact that molecules targeting the cholinergic pathway rescue some behavioral and molecular phenotypes in the FXS *Drosophila* model (Chang et al. 2008).

In addition, other pathways involving proteins encoded by poorly characterized FMRP mRNA targets are also highlighted by the network approach. First, the mRNA encoding the neuronal calcium-binding protein Calbindin1 (CALB1) was shown to bind FMRP by filter binding assay (Miyashiro et al. 2003), and we provide evidence that the interaction occurs in vivo in brain (Fig. 6). Interestingly, Calbindin1 directly targets *myo*-inositol monophosphatase (IMPA1) in spines and dendrites of cerebellar Purkinje neurons (Schmidt et al. 2005). Deregulations of CALB1 levels might, therefore, directly drive the cerebellar decrease in *myo*-inositol. Intriguingly, the *Calb1*-KO cerebellum displays the similar Purkinje cell spine dysgenesis phenotype as the *Fmr1*-KO mouse (Vecellio et al. 2000), reinforcing the potential involvement of CALB1 in FXS. Also, deficits in the neurotransmitters GABA and glutamate are connected to FMRP by pivotal mRNA targets (Fig. 5; Table 2; Supplemental Table S3) encoding, respectively, the $GABA_B$ receptor subunits GABRD and GABRP (Miyashiro et al. 2003) and the NMDA-glutamate receptor GRIN1 and GRIN2B (Schütt et al. 2009). It is interesting to underline that mutations in both *GRIN1* and *GRIN2B* are involved in forms of syndromic or nonsyndromic ID (Gecz 2010). Finally, the iMIM network highlights pivotal roles for the mRNA encoding the G-protein regulator GNAI2 (Miyashiro et al. 2003), which is involved in neuronal development (Shinohara et al. 2004), and the mRNA encoding the transcription factor Forkhead box class O3 (FOXO3), which influences behavioral processes linked to anxiety and depression (Polter et al. 2009). Our iMIM strategy usefully brings to light signaling pathways that are likely to be directly involved in the pathophysiology of FXS.

Conclusions

Our study defines for the first time a robust metabolic phenotype (metabotype) associated with *Fmr1*-deficiency, involving several neurotransmitters and the readjustment of brain biochemical pathways, suggesting that FXS may not only be a mental disease restricted to alterations in local neuronal functions but also a metabolic disease. Since FMRP affects mRNA translation and protein-protein interaction networks, we developed a network biology method which we named integrated metabolome and interactome mapping, connecting the causative mutation in *FMR1* to its metabotype via the interactome. Thus, we demonstrated that FMRP impacts a variety of transduction cascades, and metabolic and signaling pathways which could be shared with other diseases (e.g., Alzheimer's disease, other IDs). The key regulatory proteins identified by iMIM were functionally validated in vivo by UV-CLIP and constitute ideal candidate drug targets for further therapeutic development (Yildirim et al. 2007). Finally, interactome-mapping

of metabolic phenotypes is easily amenable to the study of other monogenic disorders or polygenic disorders and should contribute to understanding metabolomic signatures in various mechanistic and signaling contexts.

Methods

Animal handling and sample collection

Fmr1-knockout mice of the FBV strain and their wild-type littermates were used in this study. Genotypes were determined by PCR analysis of DNA extracted from tails, according to the original paper describing these animals (The Dutch-Belgian Fragile X Consortium 1994). The day of birth was considered as post-natal day 0. For western blot and immunohistochemistry, wild-type FVB mice were sacrificed post-natally at various time points, the brain was quickly removed from the skull and stored at −80°C for further analysis. For ^{1}H-MAS NMR analysis, the study was restricted to males aged 11–12 d. Animals were killed by cervical dislocation. The brain was then quickly removed from the skull and dissected, always in the same sequence (first cerebellum, followed by cortex, hippocampus, and striatum). These operations were typically processed within 5–10 min to limit post-mortem changes in the metabolite content of the samples. Right and left samples of each anatomical region were then immediately snapped-frozen in liquid nitrogen and stored at −80°C until further analysis. A total of n = 10 knock-out and n = 10 wild-type animals were analyzed in this study.

Western blot and immunohistochemistry

Brain samples were thawed on ice, weighed, and extracted in 2 mL/100 mg of cold extraction buffer (20 mM Tris pH 7.4, 2.5 mM $MgCl_2$, 150 mM NaCl, 0.5% NP40) supplemented with antiprotease cocktail (Roche). Lysates were sonicated on ice twice for 20 sec and centrifuged at 10,000 g for 10 min at 4°C. Supernatant was collected, and protein content was determined by spectrometry at 280 nm using Bradford reagent (Biorad). 25 μg of proteins were loaded on an 11% SDS-PAGE, and western blotting was performed as described (Davidovic et al. 2006), using the mAb1C3 anti-FMRP monoclonal antibody (Devys et al. 1993). For immunohistochemistry, a 12-d- old wild-type mouse was deeply anesthetized with isoflurane and transcardially perfused with 4% paraformaldehyde in PBS. The brain was removed, post-fixed overnight, transferred to cryoprotective solution (HistoPrep, Fisher Scientific), frozen, and serially cut into longitudinal sections (15 μm) with a Leica CM1900 cryostat. Immunohistochemistry was performed with the anti-FMRP mAb1C3 antibody revealed by DAB staining using the Vectastain Elite ABC kit, according to the manufacturer's protocol, as described (Devys et al. 1993). Sections were finally counterstained with cresyl-violet and observed with a Leica DMD108 digital microscope.

^{1}H HR-MAS NMR spectroscopy

All NMR experiments were carried out on a Bruker Avance spectrometer (Bruker GmbH) operating at 700 MHz. About 10 mg of brain tissue (1 mm^3) was filled in a HR-MAS NMR rotor and spun at 4 kHz for one-dimensional analysis with a high-resolution Magic Angle Spinning probe operating at 4°C. To record low-noise, high-resolution spectral data, samples were spun for a 25-min acquisition to accumulate 1024 transient scans. One- and two-dimensional NMR structural assignment was performed using data from the literature, HMDB (http://www.hmdb.ca/) and S-Base (Bruker GmbH).

Data import and pattern recognition

^{1}H HR-MAS NMR spectra were referenced to the center of the alanine doublet at δ1.48, phased and baseline-corrected using the Topspin 1.3 interface (Bruker GmbH). They were reduced over the chemical shift range of −0.49 to 9.59 ppm with exclusion areas around residual water signal (4.61–4.99 ppm) and its magic angle spinning side band −0.40 to –0.19 ppm) using AMIX (Bruker GmbH) to 10,000 10^{-3} ppm wide regions (buckets), and the signal intensity in each region was integrated. The corresponding bucket tables were then exported to Simca-P 12 (Umetrics), Matlab, and R for statistical analyses after row profile (constant sum) normalization.

Multivariate statistics

Principal component analyses (PCA) were run to check the homogeneity of NMR spectra and exclude outliers. Orthogonal partial least-squares discriminant analyses were run to discriminate the experimental groups of mouse brains by adding a supplementary data matrix Y, containing classification information about factors such as genetics and brain region.

Metabolite Set Enrichment Analysis

To identify the most significantly affected metabolic pathways, the metabolites affected by *Fmr1*-deficiency were analyzed by Metabolite Set Enrichment Analysis approach (Xia and Wishart 2010; Pontoizeau et al. 2011), defined as an extension of Gene Set Enrichment Analysis (Subramanian et al. 2005), to test for metabolic pathways enrichment. For each brain region and each metabolic pathway, a 2 × 2 contingency table was built by counting the corresponding number of metabolites. An exact Fisher test was then applied to statistically assess the overrepresentation of discriminant metabolites according to the whole metabolome, i.e., the whole set of metabolites assumed to exist in the brain, according to Rivals et al. (2007). To control the false discovery rate associated with multiple testing, the exact Fisher test *P*-value was finally adjusted using the Benjamini and Hochberg procedure. Only the adjusted *P*-value is presented in the tables.

Integrated metabolome and interactome mapping of *FMRI*-deficiency metabotypes

To functionally connect the *FMR1* gene deficiency in FXS to the candidate biomarker metabolites identified by OPLS-DA analysis, a bottom-up approach, combining scientific knowledge extracted from public databases and the literature, was devised to build the integrated metabolome and interactome mapping network related to *FMR1*-KO. For standardization purpose, human official genes and proteins symbols were used throughout the iMIM approach. One part of the network is composed of the *FMR1* gene and the biomarkers ligand receptors (glutamate, GABA, alanine, taurine, acetylcholine, and aspartate), but also the target enzymes known to be involved in the metabolism of the biomarkers. Lists of the 283 receptors and target enzymes linked to the 25 metabolites were extracted, respectively, from the KEGG database (Kanehisa et al. 2008) and NeuroDB, a database of receptor-ligand interactions developed by Yale University (http://senselab.med.yale.edu/NeuronDB/). To connect *FMR1* dysfunction to the 25 distinct biomarker metabolites, the network integrates metabolite-enzyme interactions (mei) based on the comprehensive metabolic network defined in KEGG but also metabolite-receptor interactions (mri) available in the comprehensive receptor-ligand database NeuroDB. *FMR1* and this set of receptors and target enzymes were next functionally connected through protein-protein interaction (ppi)

inferred from a comprehensive mammalian interactome comprising 8788 proteins and 70,897 interactions (Navratil et al. 2009). According to the functional importance of FMRP in mRNA translation regulation mediated by direct binding of FMRP to its target mRNA, the *FMR1* network was also completed with protein-RNA interactions (pri). A database of 241 interactions, including nonredundant pri ($n = 214$) and ppi ($n = 27$) between FMRP and its target mRNA or its binding partners, was extensively curated from the literature (see Supplemental Table S1 for a complete list of references). The final network includes FMR1, 42 target enzymes and three receptors, 117 target mRNAs of FMRP (encoding one enzyme SOD1 and seven receptors, notably GABRP, GABRD, and GRIK5), and 25 metabolites.

Gene Set Enrichment Analysis

Gene Set Enrichment Analysis was based on Gene Ontology (biological process) and KEGG, and the Exact Fisher's statistical procedure (Rivals et al. 2007) was used to characterize overrepresented functions associated with mRNA targets of FMRP and genes included in the FMR1 knock-out network as compared to the entire GO biological process annotation of the proteome.

Topological analysis of the iMIM knowledge network

The knowledge network was mathematically formalized as an undirected multilabeled graph Gm,n = (Vm,En) composed of three node types, Vm, where m = {"proteins," "mRNA," "metabolites"}, and four functional edges, En, where n = {"ppi," "pri," "mei," "mri"}.

A few definitions are provided as follows:

Shortest Path (sp): To understand how *FMR1*-deficiency propagates throughout the functional knowledge network, shortest paths from *FMR1* to the target enzymes associated with each candidate biomarker metabolite were measured. The shortest path problem corresponds to finding a path between two nodes such that the sum of the weights of its constituent edges is minimized. The shortest paths—also called geodesics—are computed here by using a breadth-first search in the *FMR1*-KO iMIM network. In the particular case of the iMIM network, edge weights are not used, i.e., all edge weights equal one. The shortest path length (spl) between two nodes is the distance defined by the number of hops between these two nodes within the *FMR1* knockout functional knowledge network. For example, *FMR1* is at a one-hop distance from a target enzyme if they are separated by only one edge (for instance, *FMR1* is directly connected to SOD1 by a protein-RNA interaction).

Pivotal Betweenness (pb): To quantitatively rank the importance of pivotal molecules into the interaction network, a new network metric, based on a betweenness centrality measure (Freeman 1977) was defined, called the pivotal betweenness. For each node, the betweenness [b(v)] can be defined by the number of shortest paths going through a node v and is normalized by twice the total number of protein pairs in the network [n × (n−1)].

$$b(v) = \frac{1}{n \times (n-1)} \times \sum_{i,j,v \in V} \frac{sp_{ij}(v)}{sp_{ij}}$$

In the equation used to compute the betweenness, b(v), for a node v, sp_{ij} is the number of shortest paths going from node *i* to *j*, *i* and *j* ∈ V, and $sp_{ij}(v)$ is the number of shortest paths from *i* to *j* that pass through the pivotal node. The pivotal betweenness is a particular case of betweenness, with *i* being *FMR1*, and *j* the list of target enzymes. A high pivotal betweenness value for a given molecule indicates that this pivotal molecule is highly central to the metabolic biomarker functional path.

Metabolite confirmation assays

Total proteins from *Fmr1*-KO and WT littermates were extracted from cortex and cerebellum using lysis buffer (10mM Tris pH 7.4, 5 mM EDTA, 0.1% SDS, 0.5% deoxycholate, 0.5% NP40) and quantified with a Bradford assay according to the manufacturer's recommendations (Biorad). Protein levels in each sample were further verified by Coomassie-blue staining. Glutamate levels were then quantified in 40 μg of total protein content using a glutamate enzymatic assay according to the manufacturer's protocol (BioAssay Systems). GABA levels were quantified in 100 μg of proteins using a GABA ELISA kit (Labor Diagnostika Nord). Data ($n = 9$ animals per genotype) were analyzed with a one-tailed Mann-Whitney nonparametric statistical test (*U*-test), and box plots were constructed using the Prism4 software.

UV-crosslinking and immunoprecipitation mRNA interaction confirmation assay

To isolate mRNAs associated with FMRP in vivo, UV-crosslinking and immunoprecipitations were performed with total brain extracts from 12-d-old *Fmr1*-KO and WT mice, using the protocol described previously (Ule et al. 2005), and the R60 polyclonal antibody directed against the C terminus of FMRP, whose characterization is detailed in Supplementary Material (Supplemental Fig. S1). For each assay, 10 μg of affinity-purified anti-FMRP antibody was used to immunoprecipitate 1 mg of brain lysate. Approximately 1/100th of the homogenate and 1/20th of the immunoprecipitate were loaded on an 11% SDS-PAGE gel. Proteins transferred onto a 0.45 μm nitrocellulose membrane were revealed using the mAb1C3 recognizing FMRP (Devys et al. 1993) and the 3Fx antibody recognizing both FXR1P and FXR2P (Khandjian et al. 1998). mRNA was extracted from brain homogenate and immunoprecipitates using TRIzol reagent (Invitrogen) according to the manufacturer's protocol and reverse-transcribed (RT) using the SuperscriptScriptII RT-PCR system (Invitrogen). RT products were subjected to polymerase chain reaction (PCR), using a PCR Master

Table 3. List and details of primers used to detect mRNAs associated in vivo with FMRP immunoprecipitates

Target mRNA	Primer name	5′ 3′sequence	Amplicon size	Cycle number	Reference
Fmr1	F	GCTCCAACAGAGGAAGAGGG	306 bp	$n = 35$	(Bechara et al. 2009)
	R	GGGTACTCCATTCACCAGCGG			
Mtap1b	F	TCCGATCGTGGGACACAAACCTG	228 bp	$n = 45$	(Edbauer et al. 2010)
	R	AGCACCAGCAGTTTATGGCGGG			
Sod1	F	ACCATCCACTTCGAGCAGAA	196 bp	$n = 25$	(Bechara et al. 2009)
	R	AGTCACATTGCCCAGGTCTC			
Rhoa	F	TGGTTGGGAACAAGAAGGAC	233 bp	$n = 45$	Primer3
	R	TGAGGCACCCAGACTTTTTC			
Calb1	F	GAAGGAAAGGAGCTGCAGAA	212 bp	$n = 50$	Primer3
	R	TTCCTCGCAGGACTTCAGTT			
Tubb3	F	CGAGACCTACTGCATCGACA	151 bp	$n = 35$	Primer3
	R	CATTGAGCTGACCAGGGAAT			
Pgk1	F	GAAGGGGAAGCGGGTCGTGATG	206 bp	$n = 35$	(Edbauer et al. 2010)
	R	GCAGCAACTGGCTCTAAGGAGTACTTG			

Primer sequences originated either from literature or were designed using the Primer3 webtool.

Kit (Promega) and primers, detailed in Table 3, specific for *Fmr1*, *Sod1*, *Mtap1b*, *Rhoa*, *Calb1*, *Tubb3*, and *Pgk1* mouse cDNAs. The PCR program consisted in 10 min of initial denaturation at 95°C, followed by *n* cycles of: 30 sec at 95°C, 30 sec at 58°C, 30 sec at 72°C, and a final elongation step of 10 min at 72°C. PCR products were visualized on a 1.5% TAE agarose gel, and amplicon size was verified using the 1 Kb+ DNA ladder (Invitrogen).

Acknowledgments

We thank Prof. Elaine C. Holmes, Dr. Richard H. Barton, and Dr. Josune Olave Fidalgo for their helpful comments. The authors gratefully acknowledge the excellent technical support of Ms. Nelly Durand (IPMC, CNRS UMR6097, Valbonne, France) and Ms. Giuseppina Barrancotto (IRCCS Oasi Maria SS, Troina [EN], Italy). We also thank Franck Aguila (IPMC, CNRS UMR6097, Valbonne, France) for help with Figure 7 design. L.D. is funded by the FRAXA Research Foundation and the Marie Curie European Community Program (FP6 MEIF-CT-2006-41096 and FP7-PEOPLE-ERG-2008-239290). M.V.C. is funded by Telethon (GGP07264, Italy), Ministry of Health (Italy), PRIN (Italy), and Fondation Jérôme Lejeune (France). B.B. is funded by Agence Nationale de la Recherche (the Cure-FXS project, under the FP7 E-Rare program), by Fondation pour la Recherche Médicale (Équipe FRM 2009), by Fondation Jérôme Lejeune, and by AFM. M.E.D. holds a Young Investigator Award (ANR-07-JCJC-0042-01) and grants (ANR-08-GENO-030-02, ANR-07-CP2D-SYSBIOX-18) from Agence Nationale de la Recherche.

Authors' contributions: L.D., M.V.C., B.B., and M.E.D. designed the project. L.D., M.V.C., C.M.B., and M.E.D. performed the research. L.D., V.N, and M.E.D. performed the data analysis. L.D., V.N., B.B., and M.E.D. analyzed the results. L.D. and M.E.D. wrote the paper.

References

Akerman CJ, Cline HT. 2007. Refining the roles of GABAergic signaling during neural circuit formation. *Trends Neurosci* **30:** 382–389.

Bardoni B, Davidovic L, Bensaid M, Khandjian EW. 2006. The Fragile X syndrome: Exploring its molecular basis and seeking a treatment. *Expert Rev Mol Med* **8:** 1–16.

Bassell GJ, Warren ST. 2008. Fragile X syndrome: Loss of local mRNA regulation alters synaptic development and function. *Neuron* **60:** 201–214.

Bechara EG, Didiot MC, Melko M, Davidovic L, Bensaid M, Martin P, Castets M, Pognonec P, Khandjian EW, Moine H, et al. 2009. A novel function for Fragile X mental retardation protein in translational activation. *PLoS Biol* **7:** e16. doi: 10.1371/journal.pbio.1000016.

Ben-Ari Y, Gaiarsa JL, Tyzio R, Khazipov R. 2007. GABA: A pioneer transmitter that excites immature neurons and generates primitive oscillations. *Physiol Rev* **87:** 1215–1284.

Benarroch EE. 2007. Rho GTPases: Role in dendrite and axonal growth, mental retardation, and axonal regeneration. *Neurology* **68:** 1315–1318.

Blaise BJ, Giacomotto J, Elena B, Dumas ME, Toulhoat P, Segalat L, Emsley L. 2007. Metabotyping of *Caenorhabditis elegans* reveals latent phenotypes. *Proc Natl Acad Sci* **104:** 19808–19812.

Brown V, Jin P, Ceman S, Darnell JC, O'Donnell WT, Tenenbaum SA, Jin X, Feng Y, Wilkinson KD, Keene JD, et al. 2001. Microarray identification of FMRP-associated brain mRNAs and altered mRNA translational profiles in Fragile X syndrome. *Cell* **107:** 477–487.

Bureau I, Shepherd GM, Svoboda K. 2008. Circuit and plasticity defects in the developing somatosensory cortex of FMR1 knock-out mice. *J Neurosci* **28:** 5178–5188.

Callan MA, Zarnescu DC. 2011. Heads-up: New roles for the Fragile X mental retardation protein in neural stem and progenitor cells. *Genesis* **49:** 424–440.

Chang S, Bray SM, Li Z, Zarnescu DC, He C, Jin P, Warren ST. 2008. Identification of small molecules rescuing Fragile X syndrome phenotypes in *Drosophila*. *Nat Chem Biol* **4:** 256–263.

Chelly J, Khelfaoui M, Francis F, Cherif B, Bienvenu T. 2006. Genetics and pathophysiology of mental retardation. *Eur J Hum Genet* **14:** 701–713.

Chen L, Yun SW, Seto J, Liu W, Toth M. 2003. The Fragile X mental retardation protein binds and regulates a novel class of mRNAs containing U rich target sequences. *Neuroscience* **120:** 1005–1017.

Cottingham MG, Hollinshead MS, Vaux DJ. 2002. Amyloid fibril formation by a synthetic peptide from a region of human acetylcholinesterase that is homologous to the Alzheimer's amyloid-β peptide. *Biochemistry* **41:** 13539–13547.

Cruz-Martin A, Crespo M, Portera-Cailliau C. 2010. Delayed stabilization of dendritic spines in Fragile X mice. *J Neurosci* **30:** 7793–7803.

D'Hulst C, Heulens I, Brouwer JR, Willemsen R, De Geest N, Reeve SP, De Deyn PP, Hassan BA, Kooy RF. 2009. Expression of the GABAergic system in animal models for Fragile X syndrome and Fragile X-associated tremor/ataxia syndrome (FXTAS). *Brain Res* **1253:** 176–183.

Darnell JC, Jensen KB, Jin P, Brown V, Warren ST, Darnell RB. 2001. Fragile X mental retardation protein targets G quartet mRNAs important for neuronal function. *Cell* **107:** 489–499.

Darnell JC, Mostovetsky O, Darnell RB. 2005. FMRP RNA targets: Identification and validation. *Genes Brain Behav* **4:** 341–349.

Davidovic L, Bechara E, Gravel M, Jaglin XH, Tremblay S, Sik A, Bardoni B, Khandjian EW. 2006. The nuclear microspherule protein 58 is a novel RNA-binding protein that interacts with Fragile X mental retardation protein in polyribosomal mRNPs from neurons. *Hum Mol Genet* **15:** 1525–1538.

De Filippi G, Baldwinson T, Sher E. 2005. Nicotinic receptor modulation of neurotransmitter release in the cerebellum. *Prog Brain Res* **148:** 307–320.

Devys D, Lutz Y, Rouyer N, Bellocq JP, Mandel JL. 1993. The FMR-1 protein is cytoplasmic, most abundant in neurons, and appears normal in carriers of a Fragile X premutation. *Nat Genet* **4:** 335–340.

Dölen G, Bear MF. 2008. Role for metabotropic glutamate receptor 5 (mGluR5) in the pathogenesis of Fragile X syndrome. *J Physiol* **586:** 1503–1508.

Dumas ME, Barton RH, Toye A, Cloarec O, Blancher C, Rothwell A, Fearnside J, Tatoud R, Blanc V, Lindon JC, et al. 2006. Metabolic profiling reveals a contribution of gut microbiota to fatty liver phenotype in insulin-resistant mice. *Proc Natl Acad Sci* **103:** 12511–12516.

Dumas ME, Wilder SP, Bihoreau MT, Barton RH, Fearnside JF, Argoud K, D'Amato L, Wallis RH, Blancher C, Keun HC, et al. 2007. Direct quantitative trait locus mapping of mammalian metabolic phenotypes in diabetic and normoglycemic rat models. *Nat Genet* **39:** 666–672.

The Dutch-Belgian Fragile X Consortium. 1994. Fmr1 knockout mice: A model to study Fragile X mental retardation. *Cell* **78:** 23–33.

Edbauer D, Neilson JR, Foster KA, Wang CF, Seeburg DP, Batterton MN, Tada T, Dolan BM, Sharp PA, Sheng M. 2010. Regulation of synaptic structure and function by FMRP-associated microRNAs miR-125b and miR-132. *Neuron* **65:** 373–384.

El Bekay R, Romero-Zerbo Y, Decara J, Sanchez-Salido L, Del Arco-Herrera I, Rodriguez-de Fonseca F, de Diego-Otero Y. 2007. Enhanced markers of oxidative stress, altered antioxidants, and NADPH-oxidase activation in brains from Fragile X mental retardation 1-deficient mice, a pathological model for Fragile X syndrome. *Eur J Neurosci* **26:** 3169–3180.

El Idrissi A, Trenkner E. 2004. Taurine as a modulator of excitatory and inhibitory neurotransmission. *Neurochem Res* **29:** 189–197.

Freeman LC. 1977. A set of measures of centrality based on betweenness. *Sociometry* **40:** 35–41.

Gecz J. 2010. Glutamate receptors and learning and memory. *Nat Genet* **42:** 925–926.

Gecz J, Shoubridge C, Corbett M. 2009. The genetic landscape of intellectual disability arising from chromosome X. *Trends Genet* **25:** 308–316.

Gibson JR, Bartley AF, Hays SA, Huber KM. 2008. Imbalance of neocortical excitation and inhibition and altered UP states reflect network hyperexcitability in the mouse model of Fragile X syndrome. *J Neurophysiol* **100:** 2615–2626.

Gruss M, Braun K. 2001. Alterations of amino acids and monoamine metabolism in male Fmr1 knockout mice: A putative animal model of the human Fragile X mental retardation syndrome. *Neural Plast* **8:** 285–298.

Hagerman PJ. 2008. The Fragile X prevalence paradox. *J Med Genet* **45:** 498–499.

Holmes E, Tsang TM, Tabrizi SJ. 2006. The application of NMR-based metabonomics in neurological disorders. *NeuroRx* **3:** 358–372.

Iacoangeli A, Rozhdestvensky TS, Dolzhanskaya N, Tournier B, Schutt J, Brosius J, Denman RB, Khandjian EW, Kindler S, Tiedge H. 2008. On BC1 RNA and the Fragile X mental retardation protein. *Proc Natl Acad Sci* **105:** 734–739.

Illig T, Gieger C, Zhai G, Romisch-Margl W, Wang-Sattler R, Prehn C, Altmaier E, Kastenmuller G, Kato BS, Mewes HW, et al. 2010. A genome-wide perspective of genetic variation in human metabolism. *Nat Genet* **42:** 137–141.

Kamenetz F, Tomita T, Hsieh H, Seabrook G, Borchelt D, Iwatsubo T, Sisodia S, Malinow R. 2003. APP processing and synaptic function. *Neuron* **37:** 925–937.

Kanehisa M, Araki M, Goto S, Hattori M, Hirakawa M, Itoh M, Katayama T, Kawashima S, Okuda S, Tokimatsu T, et al. 2008. KEGG for linking genomes to life and the environment. *Nucleic Acids Res* **36:** D480–D484.

Khandjian EW, Bardoni B, Corbin F, Sittler A, Giroux S, Heitz D, Tremblay S, Pinset C, Montarras D, Rousseau F, et al. 1998. Novel isoforms of the Fragile X-related protein FXR1P are expressed during myogenesis. *Hum Mol Genet* **7:** 2121–2128.
Khandjian EW, Huot ME, Tremblay S, Davidovic L, Mazroui R, Bardoni B. 2004. Biochemical evidence for the association of Fragile X mental retardation protein with brain polyribosomal ribonucleoparticles. *Proc Natl Acad Sci* **101:** 13357–13362.
Khandjian EW, Bechara E, Davidovic L, Bardoni B. 2005. Fragile X Mental Retardation Protein: Many partners and multiple targets for a promiscuous function. *Curr Genomics* **6:** 515–522.
Klein J. 2005. Functions and pathophysiological roles of phospholipase D in the brain. *J Neurochem* **94:** 1473–1487.
Lan MJ, McLoughlin GA, Griffin JL, Tsang TM, Huang JT, Yuan P, Manji H, Holmes E, Bahn S. 2009. Metabonomic analysis identifies molecular changes associated with the pathophysiology and drug treatment of bipolar disorder. *Mol Psychiatry* **14:** 269–279.
Larson J, Jessen RE, Kim D, Fine AK, du Hoffmann J. 2005. Age-dependent and selective impairment of long-term potentiation in the anterior piriform cortex of mice lacking the Fragile X mental retardation protein. *J Neurosci* **25:** 9460–9469.
Liu H, Fang F, Zhu H, Xia SA, Han D, Hu L, Lei H, Liu M. 2008. Metabolic changes in temporal lobe structures measured by HR-MAS NMR at early stage of electrogenic rat epilepsy. *Exp Neurol* **212:** 377–385.
Lu R, Wang H, Liang Z, Ku L, O'Donnell WT, Li W, Warren ST, Feng Y. 2004. The Fragile X protein controls microtubule-associated protein 1B translation and microtubule stability in brain neuron development. *Proc Natl Acad Sci* **101:** 15201–15206.
McKenna MC. 2007. The glutamate-glutamine cycle is not stoichiometric: Fates of glutamate in brain. *J Neurosci Res* **85:** 3347–3358.
Miyashiro KY, Beckel-Mitchener A, Purk TP, Becker KG, Barret T, Liu L, Carbonetto S, Weiler IJ, Greenough WT, Eberwine J. 2003. RNA cargoes associating with FMRP reveal deficits in cellular functioning in Fmr1 null mice. *Neuron* **37:** 417–431.
Navratil V, de Chassey B, Meyniel L, Delmotte S, Gautier C, Andre P, Lotteau V, Rabourdin-Combe C. 2009. VirHostNet: A knowledge base for the management and the analysis of proteome-wide virus-host interaction networks. *Nucleic Acids Res* **37:** D661–D668.
Navratil V, de Chassey B, Meyniel L, Pradezynski F, Andre P, Rabourdin-Combe C, Lotteau V. 2010. System-level comparison of protein-protein interactions between viruses and the human type I interferon system network. *J Proteome Res* **9:** 3527–3536.
Navratil V, de Chassey B, Combe CR, Lotteau V. 2011. When the human viral infectome and diseasome networks collide: Towards a systems biology platform for the etiology of human diseases. *BMC Syst Biol* **5:**13. doi: 10.1186/1752-0509-5-13.
Nicholson JK, Connelly J, Lindon JC, Holmes E. 2002. Metabonomics: A platform for studying drug toxicity and gene function. *Nat Rev Drug Discov* **1:** 153–161.
Nimchinsky EA, Oberlander AM, Svoboda K. 2001. Abnormal development of dendritic spines in FMR1 knock-out mice. *J Neurosci* **21:** 5139–5146.
Pears MR, Cooper JD, Mitchison HM, Mortishire-Smith RJ, Pearce DA, Griffin JL. 2005. High resolution 1H NMR-based metabolomics indicates a neurotransmitter cycling deficit in cerebral tissue from a mouse model of Batten disease. *J Biol Chem* **280:** 42508–42514.
Pellerin L. 2008. Brain energetics (thought needs food). *Curr Opin Clin Nutr Metab Care* **11:** 701–705.
Penagarikano O, Mulle JG, Warren ST. 2007. The pathophysiology of Fragile x syndrome. *Annu Rev Genomics Hum Genet* **8:** 109–129.
Polter A, Yang S, Zmijewska AA, van Groen T, Paik JH, Depinho RA, Peng SL, Jope RS, Li X. 2009. Forkhead box, class O transcription factors in brain: Regulation and behavioral manifestation. *Biol Psychiatry* **65:** 150–159.
Pontoizeau C, Fearnside JF, Navratil V, Domange C, Cazier JB, Fernandez-Santamaria C, Kaisaki PJ, Emsley L, Toulhoat P, Bihoreau MT, et al. 2011. Broad-ranging natural metabotype variation drives physiological plasticity in healthy control inbred rat strains. *J Proteome Res* **10:** 1675–1689.
Qiu LF, Hao YH, Li QZ, Xiong ZQ. 2008. Fragile X syndrome and epilepsy. *Neurosci Bull* **24:** 338–344.
Rivals I, Personnaz L, Taing L, Potier MC. 2007. Enrichment or depletion of a GO category within a class of genes: Which test?*Bioinformatics* **23:** 401–407.
Schmidt H, Schwaller B, Eilers J. 2005. Calbindin D28k targets myo-inositol monophosphatase in spines and dendrites of cerebellar Purkinje neurons. *Proc Natl Acad Sci* **102:** 5850–5855.
Schütt J, Falley K, Richter D, Kreienkamp HJ, Kindler S. 2009. Fragile X mental retardation protein regulates the levels of scaffold proteins and glutamate receptors in postsynaptic densities. *J Biol Chem* **284:** 25479–25487.
Shinohara H, Udagawa J, Morishita R, Ueda H, Otani H, Semba R, Kato K, Asano T. 2004. Gi2 signaling enhances proliferation of neural progenitor cells in the developing brain. *J Biol Chem* **279:** 41141–41148.
Subramanian A, Tamayo P, Mootha VK, Mukherjee S, Ebert BL, Gillette MA, Paulovich A, Pomeroy SL, Golub TR, Lander ES, et al. 2005. Gene set enrichment analysis: A knowledge-based approach for interpreting genome-wide expression profiles. *Proc Natl Acad Sci* **102:** 15545–15550.
Sung YJ, Dolzhanskaya N, Nolin SL, Brown T, Currie JR, Denman RB. 2003. The Fragile X mental retardation protein FMRP binds elongation factor 1A mRNA and negatively regulates its translation in vivo. *J Biol Chem* **278:** 15669–15678.
Swanger AS, Bassell GJ. 2011. Making and breaking synapses through local mRNA regulation. *Curr Opin Genet Dev* **21:** 414–421.
Tsang TM, Griffin JL, Haselden J, Fish C, Holmes E. 2005. Metabolic characterization of distinct neuroanatomical regions in rats by magic angle spinning 1H nuclear magnetic resonance spectroscopy. *Magn Reson Med* **53:** 1018–1024.
Ule J, Jensen K, Mele A, Darnell RB. 2005. CLIP: A method for identifying protein-RNA interaction sites in living cells. *Methods* **37:** 376–386.
Vecellio M, Schwaller B, Meyer M, Hunziker W, Celio MR. 2000. Alterations in Purkinje cell spines of calbindin D-28 k and parvalbumin knock-out mice. *Eur J Neurosci* **12:** 945–954.
Viola A, Saywell V, Villard L, Cozzone PJ, Lutz NW. 2007. Metabolic fingerprints of altered brain growth, osmoregulation, and neurotransmission in a Rett syndrome model. *PLoS ONE* **2:** e157. doi: 10.1371/journal.pone.0000157.
Westmark CJ, Malter JS. 2007. FMRP mediates mGluR5-dependent translation of amyloid precursor protein. *PLoS Biol* **5:** e52. doi: 10.1371/journal.pone.0000157.
Xia J, Wishart DS. 2010. MSEA: A web-based tool to identify biologically meaningful patterns in quantitative metabolomic data. *Nucleic Acids Res* (Suppl) **38:** W71–W77.
Yildirim MA, Goh KI, Cusick ME, Barabasi AL, Vidal M. 2007. Drug-target network. *Nat Biotechnol* **25:** 1119–1126.
Zhang Y, O'Connor JP, Siomi MC, Srinivasan S, Dutra A, Nussbaum RL, Dreyfuss G. 1995. The Fragile X mental retardation syndrome protein interacts with novel homologs FXR1 and FXR2. *EMBO J* **14:** 5358–5366.

Received October 20, 2010; accepted in revised form August 23, 2011.